Electron diffraction and high-resolution electron microscopy study of an amorphous $Pd_{82}Si_{18}$ alloy with nanoscale phase separation

Tadakatsu Ohkubo and Yoshihiko Hirotsu
The Institute of Scientific and Industrial Research, Osaka University, 8-1 Mihogaoka, Ibaraki, Osaka 567-0047, Japan
(Received 24 September 2001; revised manuscript received 9 August 2002; published 4 March 2003)

A structure model of nanoscale phase separation has been proposed for a structure of an amorphous Pd-Si alloy with the eutectic composition on the basis of electron diffraction and high-resolution electron microscopy (HREM). A sputter-deposited amorphous $Pd_{82}Si_{18}$ alloy film with a thickness of about 10 nm was specially used in order to minimize the effect of multiple scattering. A local atomic ordering with sizes of 1–2 nm was observed by HREM, similar to that observed in liquid-quenched ribbon specimens. From HREM images and nanodiffraction analysis, the atomic structure of the ordering regions was determined to be of the fcc-Pd type. Atomic pair distribution function (PDF) analysis for the thin-film alloy was performed by precise measurement of haloelectron-diffraction intensity using the imaging-plate technique. In the diffraction intensity analysis, the inelastic part of intensity was removed by an intensity correction using electron energy-loss spectroscopy. In order to explain the results of HREM, nanodiffraction, and PDF studies comprehensively, a nanoscale phase-separation structure model has been constructed with the help of reverse Monte Carlo calculation. A structure model with fcc-cluster regions embedded in a dense-random-packing structure of Pd and Si was finally obtained. The model proposed here is thought to be typical for amorphous alloys with near-eutectic compositions cooled under limited cooling rates.

DOI: 10.1103/PhysRevB.67.094201 PACS number(s): 61.14.Lj, 61.43.Dq

I. INTRODUCTION

Atomic short-range-order (SRO) structures in amorphous alloys have been analyzed mainly by x-ray and neutron atomic radial distribution function (RDF) or pair distribution function (PDF) analyses.[1,2] In these studies, atomic distances, coordination numbers, and coordination polyhedra have been mainly discussed. According to the structure analyses of amorphous alloy ribbons and films with transition-metal-metalloid (TM-M) systems, trigonal prisms formed by a central metalloid and the surrounding six metal atoms are always predominant as their SRO structures.[3] The trigonal prisms often accompany capping metal atoms on the three prism planes, and as a consequence, a nine-nearest-neighbor coordination is often realized. In recent years, atomic medium-range order (MRO) is frequently argued as being more appropriate.[3–6] The MRO structures analyzed so far from x-ray and neutron diffraction correspond to those of short-range MRO,[3] in which atomic correlation ranges over distances of about 0.3–0.5 nm. The above SRO and short-range MRO structures, however, have been so far analyzed based on the concept of homogeneous-structure systems.

We carried out high-resolution electron microscopy (HREM) studies of TM-M amorphous alloys with eutectic compositions. In an *a*-$Fe_{84}B_{16}$ (hereafter, ''*a*-'' denotes ''amorphous'') ribbon specimen, locally ordered regions as small as 1 nm with a bcc-Fe(B) structure (B is well presumed to be dissolved in the structure) were observed as local crossed-lattice fringe images under a suitable defocus condition.[7] Also in *a*-$Pd_{77.5}Cu_6Si_{16.5}$ (ribbon[8]) and *a*-$Pd_{82}Si_{18}$ (film,[9] ribbon[10]) alloys, locally ordered regions with a fcc-Pd(Si) structure were observed. A formation of local regions with atomic ordering embedded in the amorphous matrix reflecting MRO was confirmed in these amorphous alloys in spite of appearances of halo patterns in electron diffraction. These observations demonstrated that amorphous TM-M alloys with near-eutectic compositions have locally ordered regions in the form of α-phase (primary phase in crystallization) atomic structures. Such structural features were observed also in other TM-M alloys.[11] In the case of the *a*-Pd-Si alloy with the compound composition $Pd_{75}Si_{25}$, we also observed locally ordered regions and the structure was identified by nanodiffraction as that of the hexagonal Pd_2Si type.[12]

On the local structures of rapidly quenched amorphous alloys of TM-M systems with eutectic compositions studied so far, two types of local order structures, one the trigonal prism-type structure and the other the α-phase cluster-type one, were observed independently by x-ray or neutron diffraction and by HREM studies as mentioned above. The discrepancy on the local structure, which reflects SRO or MRO in the amorphous alloys studied by the different structural investigation techniques, can only be explained by introducing a structural model of nanoscale (or micro-) phase separation, where metal atom clusters (usually corresponding to those of the α-phase structure) are homogeneously distributed in the metalloid-enriched amorphous matrix composed of trigonal prisms. Such a structure with nanoscale phase separation (or this may be called nanoscale phase decomposition) is thought to be a quenched-in nonequilibrium structure leading to the development of phase separation. The structural concept of nanoscale phase separation was first introduced for *a*-Fe-B and *a*-Pd-Si alloys by Dubois and Le Caer[13] and extended by Hermann and Mattern.[14] A model called the crystal-embryo model,[15] proposed by Hamada and Fujita, which treated the growth of bcc-Fe clusters during quenching of Fe-B eutectic alloys from the melt, can be included in the concept of nanoscale phase separation. These

ideas of nanoscale phase separation in *a*-Fe-B alloys could explain Mössbauer spectra[16,17] and magnetic properties[18] well. In spite of these proposals of the structure of the amorphous TM-M systems, to our best knowledge no detailed investigation has been done that has demonstrated the nanoscale phase separation, although a nanoscale phase separation of the spinodal type has recently been demonstrated to occur in metal-metal systems, such as Ag-Ni.[19]

Our purpose in the present investigation is to demonstrate nanoscale phase separation as a realistic structural form in amorphous TM-M alloys formed under usual rapid-cooling techniques with limited cooling rates. For the demonstration, it is necessary to construct a plausible structure model to explain the details of the PDF (or the RDF). For the construction of the structure model, HREM observation is quite advantageous for details of the locally ordered regions. We took advantage of electron microscopy, which enables both the HREM observation and the PDF analysis (by electron diffraction) from the same specimen. The suitable specimen for the present purpose was a thin-film a-$Pd_{82}Si_{18}$ with a homogeneous thickness as thin as 10 nm, specially prepared to minimize the multiple scattering in selective area electron diffraction (SAED). The specimen had the same locally ordered regions as observed in usual rapidly quenched ribbon specimens. In obtaining precise electron-diffraction intensity profiles, we utilized modern electron microscopy techniques: electron energy-loss spectroscopy (EELS) to estimate the inelastic-scattering part of the intensity in electron diffraction and an imaging-plate technique for precise electron intensity recording, to obtain a precise electron-diffraction intensity profile from this alloy for the PDF analysis. In this study, a realistic nanoscale phase-separation model was constructed on the basis of HREM observation, followed by a refinement of the model using reverse Monte Carlo (RMC) calculation by comparing the calculated PDF and the experimental one obtained from the electron-diffraction intensity analysis. It was noted that precise scattering information can be obtained from electron diffraction over a wide range of scattering angles for the purpose of a precise PDF analysis.

II. EXPERIMENTAL PROCEDURES

A. Specimen preparation and structural analysis method

An amorphous thin-film specimen as thin as 10 nm with a composition of $Pd_{82}Si_{18}$ was formed on single-crystal substrates of NaCl by Ar-beam sputtering. A cast disk of $Pd_{80}Si_{20}$ alloy was used as a sputtering target. Ar sputtering was started after evacuating the chamber to $\sim 1\times 10^{-5}$ Pa by a cryopump system. The substrate temperature for the deposition was kept at 293 K during deposition using a substrate-cooling system. The specimen thickness was measured using a quartz thickness monitor and the final thickness was about 10 nm. The composition of the film specimen was determined by energy dispersive x-ray analysis with the help of reference Pd-Si amorphous ribbon samples whose compositions were analyzed in advance by electron probe microanalysis.

An HREM observation was made using a JEM-2010 transmission-electron microscope (TEM) operating at 200 kV. A nanobeam electron-diffraction study was made using a JEM-3000F TEM with a field-emission gun. Halo-diffraction patterns were taken using SAED in a JEM-2010 TEM, and the intensity recording was performed using an imaging-plate (IP) technique.[20,21] In halo-diffraction intensity analysis, EELS (Gatan-PEELS model 666) was used to estimate the inelastic part of intensity along the scattering angle.[21] In order to check the radiation damage on this specimen in HREM, we tried an HREM observation at 200 kV under different electron doses: an HREM image was taken first under a usual dose (5 pA/cm^2), and then, the same area was observed successively under a dose ten times larger than the usual one, and then the HREM image was taken. No appreciable structural difference was observed before and after the high dose.

B. PDF analysis from electron-diffraction intensity

According to diffraction theory,[1–3] a reduced interference function is defined as

$$F(Q)=[I(Q)-N\langle f^2\rangle]Q/N\langle f\rangle^2 = [I_{\mathrm{obs}}(Q)-BG(Q)]Q\langle f^2\rangle/BG(Q)\langle f\rangle^2, \quad (1)$$

where $I(Q)$ is the elastic-scattering intensity, N the total atoms concerned, and Q the scattering vector ($Q=4\pi\sin\theta/\lambda$; θ is the half scattering angle and λ, in the present case, the electron wavelength). $I_{\mathrm{obs}}(Q)$ is the observed elastic intensity and $BG(Q)$ the background intensity, which smoothly links the middle points between the intensity maxima and minima of the halo-intensity profile almost along the $\langle f^2\rangle$ curve. The square-mean and mean-square atomic scattering factors for electrons $\langle f^2\rangle$ and $\langle f\rangle^2$ are expressed as $\langle f^2\rangle=\Sigma N_j f_j^2/N$ and $\langle f\rangle^2=(\Sigma N_j f_j)^2/N^2$, where $N=\Sigma N_j$ and N_j and f_j are the atom number and atomic scattering factor (including the temperature factor) for element j, respectively. The function $F(Q)$ is related to the reduced distribution function $G(r)$ by the Fourier transform as

$$G(r)=(2/\pi)\int_0^\infty F(Q)\sin(Qr)dQ=4\pi r[\rho(r)-\rho_0], \quad (2)$$

where r is the radial distance, $\rho(r)$ the atomic density, and ρ_0 the average atomic density. The atomic PDF $g(r)=(\rho(r)/\rho_0)$ and the RDF $4\pi r^2\rho(r)$ can be obtained by $G(r)$. It should be noted that in a precise electron-diffraction PDF analysis the most important procedure is to obtain diffraction intensity profiles as close as that of kinematical intensity with less inelastic and multiple scattering, and with good linearity in intensity recording. In the case of intensity close to the kinematical one, the background $BG(Q)$ can be drawn almost along the $\langle f^2\rangle$ curve.

In the present diffraction intensity analysis, radial distortions of the diffraction patterns from the central direct spot were corrected with the help of reference Debye-Scherrer rings of Au. The inelastic-scattering part of intensity was estimated as correctly as possible along the scattering angle by taking advantage of the EELS measurement. The data

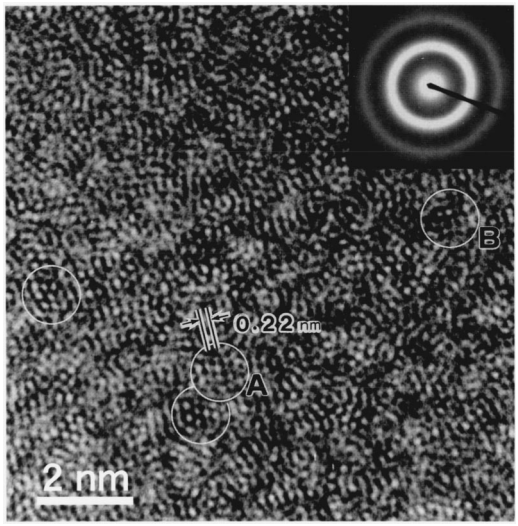

FIG. 1. HREM image of a-$Pd_{82}Si_{18}$ thin film with locally ordered regions (circled). A SAED pattern is shown in the inset.

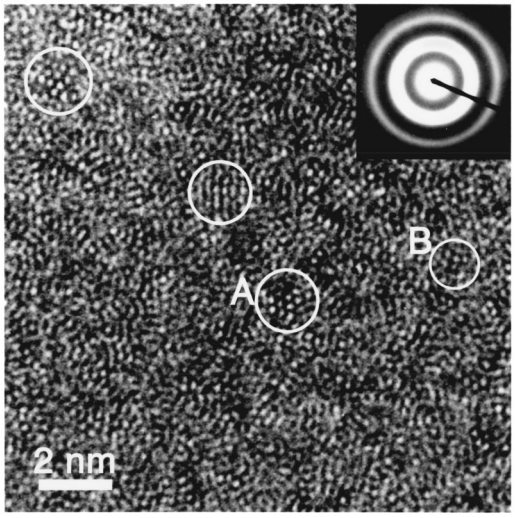

FIG. 2. HREM image taken from a rapidly quenched a-$Pd_{82}Si_{18}$ ribbon specimen showing locally extended ordered regions (circled). The specimen was thinned using ultramicrotomy. A SAED pattern is shown in the inset. The crossed-lattice fringe geometries in areas A and B resemble those of areas A and B in Fig. 1, respectively.

point of EELS along the Q vector up to $Q=120\ \mathrm{nm}^{-1}$ was 35. The details of the measurement of the inelastic intensity by EELS in the amorphous alloy specimen can be found elsewhere.[21] The ratios of elastic intensity to total intensity $I_{\mathrm{el}}(Q)/I_{\mathrm{tot}}(Q)$ could be evaluated along the scattering up to the angles $Q \leqq 120\ \mathrm{nm}^{-1}$. The ratio beyond $Q > 120\ \mathrm{nm}^{-1}$ was taken as unity, since the contribution of the inelastic intensity becomes negligible beyond the Q value. The intensity read on the IP was then digitized by laser scanner and processor. The observed intensities with the same Q value were averaged, and thus, the intensity profile $\langle I(Q)\rangle$ was obtained up to a large scattering vector Q. To obtain $\langle I(Q)\rangle_{\mathrm{el}}$ only from elastic scattering, the ratio $I_{\mathrm{el}}(Q)/I_{\mathrm{tot}}(Q)$ was multiplied by the measured $\langle I(Q)\rangle$ for each Q: $\langle I(Q)\rangle_{\mathrm{el}}$ $[=I_{\mathrm{obs}}(Q)]=\langle I(Q)\rangle[I_{\mathrm{el}}(Q)/I_{\mathrm{tot}}(Q)]$. The interference function $F(Q)$ for the elastic scattering was then obtained by drawing a background curve $BG(Q)$.

III. RESULTS

A. HREM observation and nanodiffraction

Figure 1 shows an example of the HREM image from the present thin a-$Pd_{82}Si_{18}$ film deposited on the room-temperature substrate. Regions with local lattice fringes can be seen in the encircled areas. In our previous HREM imaging of film[9] and ribbon[10] a-$Pd_{82}Si_{18}$ alloys, we frequently observed such locally ordered regions of α-Pd(Si) clusters as lattice fringe regions extending as small as 1–2 nm. An example of such HREM imaging from the liquid-quenched a-$Pd_{82}Si_{18}$ ribbon specimen is also shown in Fig. 2 for comparison. The crossed-lattice fringe geometries of the local regions in the encircled areas A and B are the same as those observed in areas A and B in Fig. 1 of the present thin-film specimen. The HREM images of Figs. 1 and 2 were taken using a 200-kV TEM.

The observation condition of the locally ordered regions was based on the ''defocus method,'' [10] which enables lattice imaging of localized crystalline atomic clusters embedded in an amorphous matrix taking advantage of the Fourier image related to the phase-contrast transfer function.[22] The extension of the clearly observed crossed-lattice fringe regions in Fig. 1 ranges from about 1 to 1.6 nm. According to our image simulation of fcc-Pd(Si) clusters embedded in the dense randomly packed (DRP) structure of Pd and Si atoms (thickness: 3.3 nm), a cluster region with a diameter of 2 nm can be imaged as lattice images extending to as small as about 1.5 nm due to the disturbance of the image by the surrounding DRP structure.[10] Therefore, the real average size of the locally ordered regions in the present a-$Pd_{82}Si_{18}$ film must be between ~1.5 and 2 nm. Regarding the distribution of the locally ordered regions, random distributions both in position and orientation can be expected from the HREM images. The volume fraction of the HREM regions is thought to be well below 40%, by reference to the result of image simulation.[10] In SAED, a halo pattern is observed (as seen in the insets in Figs. 1 or 2). Examples of nanodiffraction patterns from such locally ordered regions in the sputtered thin-film specimen are shown in Figs. 3(a) and 3(b). They were taken using the 300-kV TEM with a field-emission gun. The

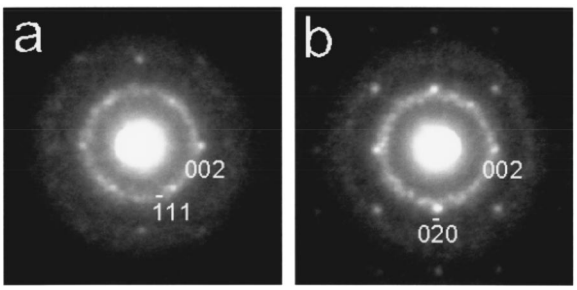

FIG. 3. Nanodiffraction zone-axis [110] (a) and [100] (b) patterns from the fcc-Pd(Si) cluster regions in the a-$Pd_{82}Si_{18}$ thin film.

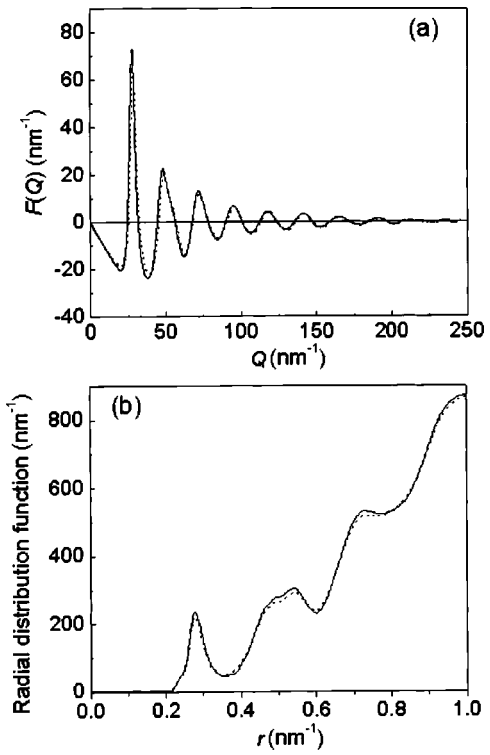

FIG. 4. Reduced interference function (a) and RDF (b) profiles obtained from electron-diffraction intensity analysis for a-$Pd_{82}Si_{18}$ thin films. In each figure, the solid line is obtained from the elastic scattering and the dotted line from the total scattering, which includes the inelastic scattering.

probe size was about 1 nm. The obtained structural information of the locally ordered regions from nanodiffraction is consistent with that from the HREM images with respect to the fringe spacings and their cross angles. The patterns in Figs. 3(a) and 3(b) correspond to those of [110] and [100] zone axes of fcc clusters, respectively. The average lattice parameter of the fcc clusters measured for ten nanodiffraction patterns was 0.402 nm with an error of $\pm 0.4\%$, which is a little larger than that of pure Pd (0.389 nm). Here, lattice plane spacings for nanodiffraction spots were measured by reference to the peak position of the first halo diffraction. The halo pattern was formed by changing the probe size to a larger one (more than 30 nm) under the same camera length as that used in nanodiffraction. From the nanodiffraction and the lattice-parameter measurement, it was concluded that the locally ordered regions are fcc-Pd(Si) clusters including Si atoms also at the interstitial sites, although the substitutional sites are favorable for Si atoms in Pd.

B. Electron-diffraction PDF profile

Figure 4(a) shows the $F(Q)$ profile for the a-$Pd_{82}Si_{18}$ thin-film specimen deposited on the room-temperature substrate. The profile was obtained from SAED up to a high-Q-value range, as high as 240 nm^{-1}. The solid line corresponds to the elastic scattering, and the dotted line to the total scattering without correction for the elastic scattering. A small difference between the two $F(Q)$ profiles appears at or near the first and second intensity peaks. By the Fourier transform of Eq. (2), the reduced RDF, $G(r)$ [Eq. (2)], was calculated. Since the drawing of the $BG(Q)$ curves to obtain the $F(Q)$ profiles were made as precisely as possible, the $G(r)$'s have almost no ripples in the regions $r<0.2$ nm. The PDF's and RDF's were then calculated using $G(r)$. The final RDF profiles obtained from $F(Q)$'s in Fig. 4(a) are shown in Fig. 4(b). The solid line is obtained from the elastic scattering, and the dotted line from the total scattering, which includes inelastic scattering. There is a small difference between the two profiles. It is noted that beside the first main peak of Pd-Pd correlation there appears a small subsidiary intensity rising at $r\sim 0.24$ nm, which corresponds to the Pd-Si correlation. These PDF profiles are similar to that obtained from neutron diffraction[23] for the a-$Pd_{80}Si_{20}$ alloy. In Table I, the structural data obtained from the present electron diffraction are shown as an average a-$Pd_{82}Si_{18}$ structure together with the corresponding reference data from neutron diffraction for a-$Pd_{80}Si_{20}$.[23] In the table, data obtained from electron diffraction without the correction for elastic scattering are also listed. In obtaining coordination numbers from the RDF, the log-normal profile fitting was applied for Pd-Pd and Pd-Si correlation peak profiles. In estimating coordination numbers, the value of the average atomic density was taken from the value for the ribbon specimen[23] with the same composition. It is noted that the atomic distances and the coordination numbers are almost equal to those obtained by neutron diffraction. It is also noted that the Pd coordination with the central Si (a partial atomic correlation) can be obtained by precise electron-diffraction intensity analysis. The structural data in Table I is evidence of a predominant formation of a trigonal SRO structure with six Pd coordinated Pd-Si prisms with respect to the central Si atoms as an average structure.

TABLE I. Atomic distances and coordination numbers obtained from the present experimental RDF analysis. Data analyzed from the electron-diffraction intensity profile including inelastic intensity are also shown. Neutron-diffraction data (Ref. 23) for a-$Pd_{80}Si_{20}$ are listed for comparison.

		Atomic distance (nm)	Coordination number
Elastic intensity	Pd-Pd	0.272	11.0
	Pd-Si	0.240	1.2
	Si-Pd		5.6
With inelastic intensity	Pd-Pd	0.274	10.7
	Pd-Si	0.241	1.8
	Si-Pd		8.0
Neutron-diffraction data $Pd_{80}Si_{20}$[a]	Pd-Pd	0.280	10.6
	Pd-Si	0.242	1.6
	Si-Pd		6.6

[a]Reference 23.

The real structure of the present amorphous alloy deposited on the room-temperature substrate includes fcc-Pd-type atomic clusters, such as in the case of a-Pd-Si ribbon specimens, though not densely formed, according to the HREM

study. So, a comprehensive structure model for this amorphous Pd-Si alloy has to be established by which both the diffraction and HREM data can be explained satisfactorily. The obtained PDF profile based on the elastic-scattering intensity was used for the following structural modeling of the present alloy. In electron diffraction, the multiple-scattering effect must be taken into account in the intensity analysis. According to our diffraction intensity simulation for an amorphous Pd-Si structure model, the effect under the acceleration voltage of 200 kV became almost negligible when the specimen thickness was less than about 15 nm (the thickness of the present specimen is about 10 nm).[24]

IV. STRUCTURE MODELING AND RMC SIMULATION

A. Initial structure model

From the above HREM, SAED, and nanodiffraction studies, we can say that a phase separation on a nanometer scale occurs in the amorphous $Pd_{82}Si_{18}$ specimen. In order to make the nanoscale phase-separation structure model by the help of RMC calculation, we prepared the initial structure model for the a-$Pd_{82}Si_{18}$ structure as the first step. In the initial structure modeling, we took such a realistic structural scheme that regions with fcc clusters were embedded in a DRP-like matrix formed by Pd and Si atoms. For the matrix structures, the SRO (trigonal prism) formation and the short-range MRO formation of trigonal prisms,[23,25] which have been argued in x-ray and neutron-diffraction studies of amorphous TM-M alloys, were ignored for convenience as the initial structure. The reason is that the SRO and the short-range MRO formations must be automatically introduced in the DRP area during the RMC calculation processes to reproduce the PDF profiles of the alloy. The fcc-cluster size, the fraction of atoms (A_f) forming the fcc clusters in the structure model, and the Si content in the fcc clusters are all important parameters and are taken in the present initial structure modeling by reference to the present HREM and nanodiffraction studies.

As initial basic structures, A_f's were taken in different combinations: $A_f=0$ (DRP model), 0.1, 0.2, and 0.3. Since the atomic volume of Pd (0.0147 nm^3) and the average atomic volume of the compound Pd_3Si (0.0142 nm^3) (Ref. 26) are almost the same, we may think that the atomic and the volume fraction of the fcc clusters can take almost the same value in the Pd-Si alloy system. For the Si composition in the fcc clusters, three compositions 0, 9, and 18 at. % were chosen. For Si sites in the clusters, half the Si atoms were at the octahedral interstitial sites formed by Pd atoms and the rest of the Si atoms were at the substitutional sites of Pd. All of these Si atoms were distributed randomly on these sites. The shape of the fcc cluster was chosen to be spherical. The fcc-cluster size was chosen to be 1.9 nm in diameter according to the average size estimation by HREM (the radius defined here is between the cluster center to the atom center of the outermost atomic shell). After the Si occupation in the clusters, energy of the clusters was minimized by way of the static structure relaxation assuming Lennard-Jones (L-J) -type interatomic potentials for Pd and Si.[27] After the relaxation, the clusters were randomly distributed with random orientations in a structure cell ($3.305\times3.305\times3.305$ nm) under the defined A_f ratio. The lattice parameters of the relaxed fcc-cluster models are between 0.400 and 0.407 nm, which are as close as those measured using nanodiffraction patterns. In each of the structure model, after placing the fcc clusters in the structure cell, the open space among the clusters was filled with Pd and Si atoms randomly by taking both the total atomic composition and the density into consideration. The obtained matrix structure was also relaxed energetically with the L-J potentials excluding the fcc-cluster regions. Before starting the RMC calculation, the total structure was finally relaxed energetically in a slight manner, in order to relax especially the structural boundaries between the cluster and the matrix. The density of the model structure was chosen to be 10.61 g/cm^3 by interpolating the experimental densities of the amorphous Pd-Si alloys.[23] The total number of atoms in each initial structure model was 2500. In Fig. 5, an example of the relaxed initial structure model is illustrated, where some fcc-Pd(Si) clusters can be partly seen.

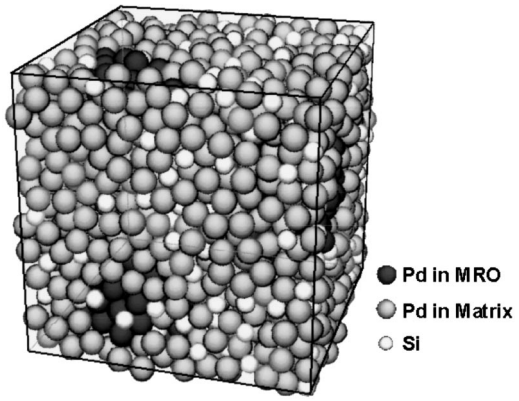

FIG. 5. An example of the schematic initial structure model. fcc-Pd(Si) clusters are embedded in the DRP Pd-Si atoms. Smaller bright spheres correspond to Si atoms. Pd atoms included in the fcc clusters can be identified as larger dark spheres.

B. RMC simulation

The RMC simulation has now become a general method for modeling the structure of disordered materials based on experimental diffraction data without any assumption of atomic interaction.[25,28] In the present RMC simulation, the atoms in the fcc-cluster regions were all fixed and only the atoms in the matrix region were moved. The lower limit of the interatomic distances in the matrix regions were chosen to be 0.245 for Pd-Pd and 0.200 nm for Pd-Si and Si-Si. The maximum value of atomic displacement in a single calculation step in the simulation was limited to 0.023 nm. The simulation consists of choosing atoms at random and moving them in arbitrary directions with arbitrary amounts. In the present calculation, an event of the atomic positional movement was accepted to be preferable only if the move resulted in a decrease of the mean-square deviation χ^2 between $g_{\mathrm{exp}}(r)$ and $g_{\mathrm{cal}}(r)$ within the radial distance $0<r\leqslant r_{\max}$

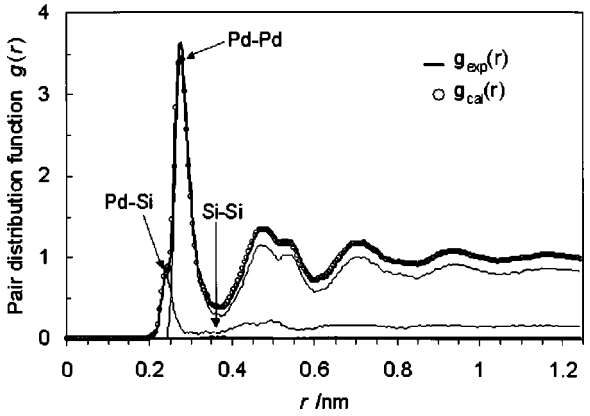

FIG. 6. Profile fitting for the total $g_{\mathrm{exp}}(r)$ and $g_{\mathrm{cal}}(r)$ for a-$Pd_{82}Si_{18}$. The fitting is for the model of $A_f=0.1$ with the Si content of 18% in the fcc cluster with the fcc-cluster size of 1.9 nm.

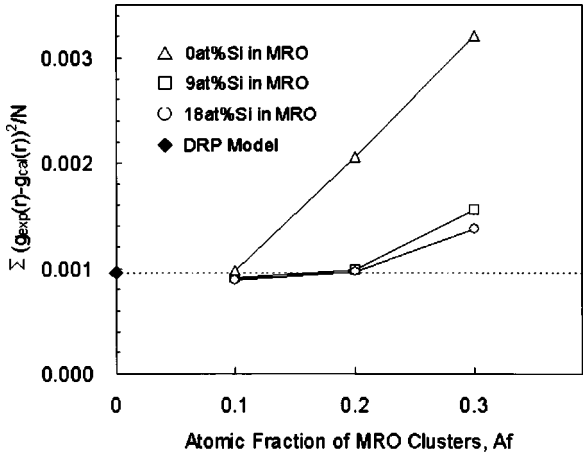

FIG. 7. Final mean-square deviations in the RMC calculation for several structural models of a-$Pd_{82}Si_{18}$ with different atomic fractions A_f to form fcc clusters and with different Si contents in the fcc cluster.

($r_{\max}$ is the maximum value of r taken in the calculation $r_{\max}$:1.25 nm). Here, χ^2 was defined as[25]

$$\chi^2=\Sigma(g_{\mathrm{exp}}(r)-g_{\mathrm{cal}}(r))^2/N, \tag{3}$$

where $g_{\mathrm{exp}}(r)$ is the experimentally determined PDF, $g_{\mathrm{cal}}(r)$ the calculated PDF, and N the number of data points. In determining a preferable atomic structure by RMC simulation, the criterion that χ^2 can be minimized for a structure model with suitable structural parameters was adopted. This criterion has been taken, for example, to determine the correct density of material.[28]

When the iteration in the RMC simulation for reducing the χ^2 value approaches the final stage, the chance of acceptance of an atomic movement becomes very small. In this calculation, when the chance of acceptance of atomic movement approached 7% per atom on average, the corresponding χ^2 value was judged to be the final one. The final iteration number was as large as 55 000–80 000 depending on the structural model. The χ^2 value was reduced exponentially in all cases. After obtaining a preferable structure model, we further examined the local structure using the Voronoi-polyhedra analysis.[29]

V. POSSIBLE STRUCTURE DEDUCED FROM RMC SIMULATIONS

An example of the profile fitting of the experimental PDF of a-$Pd_{82}Si_{18}$ by the RMC-simulated PDF is shown in Fig. 6 for the structure model with the atomic fraction $A_f=0.1$. In the figure, the total and the partial PDF's are shown. The Si content in the fcc clusters was 18 at. %. The fitting reaches the experimental PDF profile very closely in a wide range of radial distances. Under different combinations of the Si content in the cluster and A_f, the RMC simulations were performed. The results are shown in Fig. 7. The final χ^2 values for different structural models are plotted as a function of A_f. The final χ^2 values for $A_f=0$, which is for the DRP model, are also plotted. The five nanoscale phase separation structure models with the parameters (Si in fcc cluster: 0 at. %; fcc-cluster size: 1.9 nm; $A_f=0.1$), (Si in fcc cluster: 9 at. %; fcc-cluster size: 1.9 nm; $A_f=0.1$, 0.2), and (Si in fcc cluster: 18 at. %; fcc-cluster size: 1.9 nm; $A_f=0.1$, 0.2) have the final χ^2 values as small as or less than that of the DRP structure model. The minimum χ^2 value was obtained by the model with (Si in fcc cluster: 9 at. %, $A_f=0.1$) and (Si in fcc cluster: 18 at. %, $A_f=0.1$).

From Fig. 7 and also from the HREM result, the a-$Pd_{82}Si_{18}$ alloy is judged to have A_f close to about 0.1–0.2. The larger lattice distortion of fcc clusters with Si and the smaller A_f are found to be important factors for the good fit between the experimental and the simulated PDF's. The obtained range of A_f is within a plausible range according to a phase balance consideration between the amorphous phase and the primary α-phase on the basis of free-energy functions. Since it was known from an *in situ* observation[9] that the fcc clusters in the a-$Pd_{82}Si_{18}$ alloy transform into the α-phase by way of coalescence of the clusters in the primary crystallization process, the A_f value of the clusters must be less than the atomic fraction of the α phase ($A_f^{\alpha 1}$) in the primary crystallization. According to the free-energy consideration[30] and the phase diagram,[31] the value of $A_f^{\alpha 1}$ must be close to or a little less than that of the α phase in equilibrium with the orthorhombic Pd_3Si phase in the final crystallization stage ($A_f^{\alpha 2}$), namely, $A_f^{\alpha 1}\leqslant A_f^{\alpha 2}=0.28$. Figure 8 shows a set of calculated HREM images for the RMC-simulated nanoscale phase-separation model: $A_f=0.1$, 18 at. % Si in fcc clusters, and the fcc-cluster size of 1.9 nm. The figure is composed of four images for four different structures with a variety of fcc-cluster positions and orientations chosen randomly but with the same structure model parameters. This set of images can be taken as a simulated HREM image of a structure area as wide as 6.6×6.6 nm embedding the fcc clusters. The simulation was done on the basis of the multislice method[32] with a thickness of 10 nm under the same imaging condition taken in the experiment. Since the fcc-Pd(Si) clusters with the size of 1.9 nm are randomly distributed under the atomic fraction of 10% (totally, 12 fcc clusters in the four models), we have few chances to observe the fcc-lattice images from the clusters.

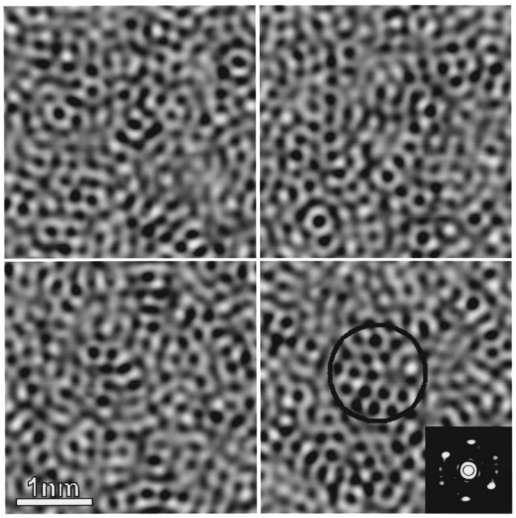

FIG. 8. Simulation of HREM image for the structure model with $A_f = 0.1$, 18% Si (in the fcc cluster), and an fcc-cluster size of 1.9 nm. Four simulated images are shown, which are based on the same structure model parameters but on a variety of fcc-cluster positions and orientations. An fcc-cluster region observed is shown in the circled area.

In the circled area of Fig. 8, the fcc-lattice region with the ⟨110⟩ zone axis can be seen. A power spectrum taken from the circled area is shown in the inset. By comparing the simulated and observed HREM images in a visual manner, it has been demonstrated that the simulated HREM images based on the structure model with the cluster volume fraction of about 10% almost corresponds to the observed structure by HREM.

In order to investigate atomic local structures, especially in the matrix region surrounding the fcc clusters, the Voronoi-polyhedral analysis has been performed using the RMC-simulated structure model. Figure 9 shows the analyzed local polyhedral structures surrounding Si atoms in the matrix for a RMC-simulated structure model with the structural conditions $A_f = 0.1$, and Si content in fcc cluster $= 18$ at. %. In the figure, types of polyhedra, expressed by the Voronoi indices, and their fractions are shown. It is noted that in the DRP-matrix structure with the volume fraction of about 90% such basic structural units as nine coordinated trigonal prisms and ten coordinated Archimedian antiprisms are predominant (the atomic structures are schematically drawn in the figure). Other Voronoi polyhedra with frequencies larger than 2% are mostly of deformed prism structures. The observed prism-related local matrix structures are consistent with the SRO structures investigated by neutron and x-ray diffraction.[23,25,27] The frequent appearance of the above types of polyhedra was also confirmed in other plausible structure models with different structural parameters. In Table I the experimentally obtained average coordination number of Pd with respect to the central Si was close to six, giving a local structural scheme of six coordinated Pd-Si prisms. On the other hand, nine coordinated or ten coordinated prism-related polyhedral structures with the central Si atoms were revealed by the RMC simulation as the main SRO structures of the matrix in the specimen (see Fig. 9).

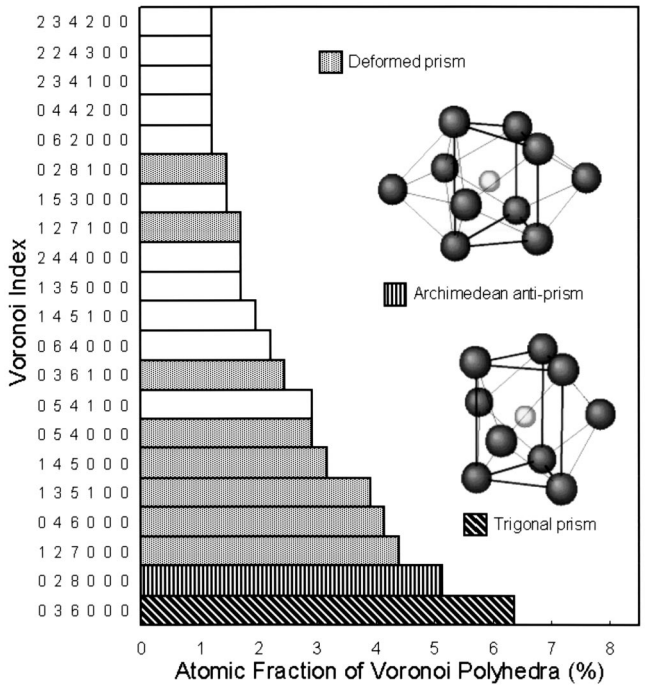

FIG. 9. Frequency histogram of Voronoi polyhedra in the DRP-matrix structure of the simulated structure model for a-$Pd_{82}Si_{18}$. In the model the Si content in the fcc cluster and A_f are 18 at. % and 0.1, respectively. Atomic arrangements of trigonal and Archimedian antiprism structures are schematically drawn in the figure.

The atomic distances between the central Si and the capping Pd atoms, which form half octahedra on the sides of trigonal prism, are slightly larger than those between the central Si and prism corner Pd atoms. The small tail in the RMC-simulated Pd-Si subsidiary peak in the RDF (see Fig. 6) extending to $r \sim 0.3$ nm must be closely related to the atomic correlations between Si and the capping Pd atoms. It is reasonable to think that the nine coordinated prism-related Pd-Si polyhedra found in the RMC-simulated structure simply come from the limiting range of near-neighbor atomic distance in the Voronoi analysis. In the present Voronoi analysis, the atomic distance limit taken for finding that type of polyhedra was 0.32 nm.

VI. CONCLUDING REMARKS

In the amorphous $Pd_{82}Si_{18}$ thin film, local atomic ordered regions were observed by HREM as in the case of the liquid-quenched amorphous $Pd_{82}Si_{18}$ alloy, in spite of observations of halo patterns in SAED. From nanodiffraction, the atomic arrangement of the locally ordered regions in the amorphous $Pd_{82}Si_{18}$ structure was confirmed to be that of the fcc-Pd-type structure. In order to explain these experimental structural features comprehensively, a nanoscale phase separation model was introduced. A suitable structure model with regions of crystalline atomic clusters embedded in a DRP structure of Pd and Si was finally obtained for the amorphous alloy with the help of reverse Monte Carlo calculation, which could explain the experimental PDF satisfactorily. It has been demonstrated that nanoscale phase separation in

this amorphous alloy occurs in such a way that the phase valance for the primary crystallization is realized approximately on nanometer scale already in the as-formed state.

The obtained structure model includes fcc-Pd(Si) clusters with a volume fraction as small as 10%–20%, and the rest of the cluster volume is composed of a DRP-like matrix region with trigonal Pd-Si prisms. The prism-related matrix region with a volume fraction as large as 80%–90% definitely contributes to the main scattering volume in x-ray or neutron diffraction. The crystalline atomic cluster regions, on the other hand, turn out to be minor volumes in diffraction. This is why structural analyses of *a*-Pd-Si alloys by x-ray or neutron diffraction always deal with only chemical SRO's or short-range MRO's with trigonal prisms. It is presumed that not only *a*-Pd-Si but also *a*-Fe-B alloys with near-eutectic composition possibly have the structure proposed here, which can explain not only the results of diffraction studies[28,29] but also the results of magnetic[30–34] and HREM (Ref. 7) studies.

In many amorphous alloys including the Pd-Si alloys, atomic density fluctuations have been observed by x-ray or neutron small-angle scattering studies.[35,36] The density fluctuations generally occur with a spatial wavelength of about 2–2.5 nm. In the case of a-$Pd_{80}Si_{20}$,[36] the length is about 2.5 nm, which is nearly equal to the average distance of the fcc clusters in our present structure model of a-$Pd_{82}Si_{18}$: for example, they are about 3 and 2.2 nm in the models with $A_f = 0.1$ and 0.2, respectively. It can be said that the density fluctuations observed by x-ray or neutron diffraction are thought to be mainly related to the nanoscale phase separation. The local structural deviation from DRP structure with local atomic compositional fluctuation in as-formed amorphous alloys was already shown using molecular-dynamics simulation,[37] and the density fluctuation was discussed in relation to small-angle scattering data.

In the present study, the experimental PDF was used to determine the approximate volume fraction of the fcc-Pd(Si) clusters in the nanoscale phase separation model with knowledge of the average cluster size and structure from HREM and nanodiffraction. Since the PDF is not so sensitive to a local structural variation, we cannot evaluate the further detailed volume fraction of the fcc-Pd(Si) clusters. For a detailed study in determining the volume fraction of local crystalline regions in the amorphous structure, other useful techniques must be introduced. Fluctuation microscopy[38] will be a candidate to extract structural and volume fraction information with MRO in such an amorphous structure as shown in this study.

ACKNOWLEDGMENTS

This work was partly supported by a Grant-in-Aid for Scientific Research from the Ministry of Education, Science, and Culture of Japan, and was also supported by Special Coordination Funds for Promoting Science and Technology on ''Nanohetero Metallic Materials'' from the Science and Technology Agency.

[1] J. F. Sadoc and J. Dixmier, Mater. Sci. Eng. **23**, 187 (1976).
[2] Y. Waseda, *The Structure of Non-Crystalline Materials, Liquids and Amorphous Solids* (McGraw-Hill, New York, 1980), p. 87.
[3] S. R. Elliott, *Physics of Amorphous Materials* (Wiley, New York, 1990), p. 71.
[4] P. H. Gaskell, J. Non-Cryst. Solids **75**, 329 (1985).
[5] J. Sietsma and B. J. Thijsse, J. Non-Cryst. Solids **101**, 135 (1988).
[6] K. Suzuki and T. Fukunaga, J. Alloys Compd. **194**, 303 (1993).
[7] Y. Hirotsu and R. Akada, Jpn. J. Appl. Phys., Part 2 **23**, L478 (1984).
[8] Y. Hirotsu, M. Uehara, and M. Ueno, J. Appl. Phys. **59**, 3081 (1986).
[9] K. Anazawa, Y. Hirotsu, and Y. Inoue, Acta Metall. Mater. **42**, 1997 (1994).
[10] Y. Hirotsu, T. Ohkubo, and M. Matsushita, Microsc. Res. Tech. **40**, 284 (1998).
[11] Y. Zhang, K. Hono, A. Inoue, A. Makino, and T. Sakurai, Acta Metall. Mater. **44**, 1497 (1995).
[12] M. Matsushita, Y. Hirotsu, T. Ohkubo, and T. Oikawa, J. Electron Microsc. **45**, 105 (1996).
[13] J. M. Dubois and G. Le Caer, J. Phys. Colloq. **C9**, 67 (1982).
[14] H. Hermann and N. Mattern, J. Phys. F: Met. Phys. **16**, 131 (1986).
[15] T. Hamada and F. E. Fujita, in *Proceedings of Rapidly Quenched Metals IV*, 1981, edited by T. Masumoto and K. Suzuki (Japanese Institute of Metals, Sendai, 1981), Vol. 1, p. 319.
[16] T. Kemeny, I. Vincze, B. Fogarassy, and S. Arajs, Phys. Rev. B **20**, 476 (1979).
[17] R. Ohshima and F. E. Fujita, Jpn. J. Appl. Phys. **20**, 1 (1981).
[18] R. Hasegawa and R. Ray, J. Appl. Phys. **50**, 1586 (1979).
[19] J. H. He and E. Ha, Phys. Rev. B **64**, 144206 (2001).
[20] N. Mori, T. Oikawa, Y. Harada, and J. Miyahara, J. Electron Microsc. **39**, 433 (1990).
[21] M. Matsushita, Y. Hirotsu, K. Anazawa, T. Ohkubo, and T. Oikawa, Mater. Trans., JIM **36**, 822 (1995).
[22] J. C. H. Spence, *Experimental High-resolution Electron Microscopy* (Clarendon, Oxford, 1981), Sect. 6, p. 193.
[23] T. Fukunaga and K. Suzuki, Sci. Rep. Res. Inst. Tohoku Univ. A **29**, 153 (1981).
[24] T. Ohkubo and Y. Hirotsu (unpublished).
[25] P. A. Duine, J. Sietsuma, B. J. Thijsse, and L. Pusztai, Phys. Rev. B **50**, 13 240 (1994).
[26] B. Aronsson and A. Nylund, Acta Chem. Scand. (1947-1973) **14**, 1011 (1960).
[27] J. M. Dubois, P. H. Gaskell, and G. Le Caer, Proc. R. Soc. London, Ser. A **402**, 323 (1985).
[28] B. O'Malley, I. Snook, and D. McCulloch, Phys. Rev. B **57**, 14 148 (1998).
[29] T. Kondo and K. Tsumuraya, J. Chem. Phys. **94**, 8220 (1991).
[30] U. Mizutani, *Progress in Materials Science* (Pergamon, New York, 1983), Vol. 28, p. 97.
[31] T. B. Massalski, *Binary Alloy Phase Diagrams*, 2nd ed. (Ameri-

can Society for Metals, Metals Park, OH, 1990), Vol. 3, p. 3045.
[32] J. M. Cowley, *Diffraction Physics* (North-Holland, Amsterdam, 1981), Chap. 11.
[33] E. Nold, P. Lamparter, H. Olbrich, G. Rainer-Harbach, and S. Steeb, Z. Naturforsch. A **36A**, 1032 (1981).
[34] G. Faigel and E. Svab, *Proceedings of Rapidly Quenched Metals V*, edited by S. Steeb and H. Warlimont (North-Holland, Amsterdam, 1985), Vol. 1, p. 487.
[35] K. Osamura, K. Shibue, R. Suzuki, Y. Murakami, and S. Takayama, J. Mater. Sci. **16**, 957 (1981).
[36] T. Fukano, K. Doi, I. Minato, and H. Hashizume, Rep. Res. Lab. Eng. Mater., Tokyo Inst. Technol. **12**, 35 (1987).
[37] C. Hausleitner, J. Hafner, and C. Becker, Phys. Rev. B **48**, 13 119 (1993).
[38] M. M. J. Treacy, J. M. Gibson, and J. Keblinski, J. Non-Cryst. Solids **231**, 99 (1998).